Imaging of Chemotherapy-Induced Acute Cardiotoxicity with ^{18}F-Labeled Lipophilic Cations

Stuart P. McCluskey[1,2], Anna Haslop[1], Christopher Coello[2], Roger N. Gunn[2,3], Edward W. Tate[1], Richard Southworth[4], Christophe Plisson[2], Nicholas J. Long[1], and Lisa A. Wells[2]

[1]Department of Chemistry, Imperial College London, London, United Kingdom; [2]Invicro LLC, London, United Kingdom; [3]Division of Brain Sciences, Imperial College London, Imperial College Centre for Drug Discovery Science, London, United Kingdom; and [4]Biomedical Engineering and Imaging Sciences, King's College London, London, United Kingdom

Many chemotherapy agents are toxic to the heart, such that increasing numbers of cancer survivors are now living with the potentially lethal cardiovascular consequences of their treatment. Earlier and more sensitive detection of chemotherapy-induced cardiotoxicity may allow improved treatment strategies and increase long-term survival. Lipophilic cation PET tracers may be suitable for early detection of cardiotoxicity. This study aimed to evaluate an ^{18}F-labeled lipophilic phosphonium cation, [1-(2-^{18}F-fluoroethyl),1*H*[1,2,3]triazole-4-ethylene]triphenylphosphonium bromide (^{18}F-MitoPhos), as a cardiac imaging agent, comparing it with leading PET and SPECT lipophilic cationic tracers before further assessing its potential for imaging cardiotoxicity in an acute doxorubicin model. **Methods:** Cardiac uptake and response to decreased mitochondrial membrane potential of ^{18}F-MitoPhos and ^{99m}Tc-sestamibi were tested in isolated perfused rat hearts. Baseline pharmacokinetic profiles of ^{18}F-MitoPhos and ^{18}F-fluorobenzyltriphenylphosphonium and their response to acute doxorubicin-induced cardiotoxicity were assessed in rats in vivo (10, 15, or 20 mg of doxorubicin per kilogram, intravenously, 48 h beforehand). **Results:** Cardiac retention of ^{18}F-MitoPhos was more than double that of ^{99m}Tc-sestamibi in isolated perfused rat hearts. A favorable biodistribution of ^{18}F-MitoPhos in vivo was observed, with heart-to-tissue ratios of 304 ± 186, 11.2 ± 1.2, and 3.8 ± 0.6 for plasma, liver, and lung, respectively (60 min). A significant dose-dependent loss of cardiac retention of ^{18}F-MitoPhos was observed on doxorubicin treatment, with average cardiac SUV from 30 to 60 min (mean ± SD) decreasing from 3.5 ± 0.5 (control) to 1.8 ± 0.1 (doxorubicin, 20 mg/kg). Other assessed biomarkers showed no alterations. **Conclusion:** ^{18}F-MitoPhos showed pharmacokinetic parameters suitable for cardiac imaging. A significant dose response of cardiac uptake to doxorubicin treatment was observed before detectable biomarker alterations. ^{18}F-MitoPhos is therefore a promising tracer for imaging chemotherapy-induced cardiotoxicity. To our knowledge, this is the first demonstration of radiolabeled lipophilic cations being used for the PET imaging of chemotherapy-induced cardiotoxicity and indicates the potential application of these compounds in this area.

Key Words: phosphonium cations; ^{18}F radiochemistry; PET; cardiotoxicity; doxorubicin

J Nucl Med 2019; 60:1750–1756
DOI: 10.2967/jnumed.119.226787

Long-term cancer survival rates are increasing, with the more-than-5-y survival rate rising from 49% for diagnoses made in the mid-1970s to 69% for diagnoses made in 2005–2011, in the United States (*1*). However, many cancer treatments are not themselves benign, and the long-term effects of cancer treatment are increasingly having an impact on patient morbidity and mortality. Doxorubicin is a widely used and effective anthracycline chemotherapy agent in a variety of cancers (*2,3*). Its therapeutic potential, however, is limited by severe and potentially lethal cardiotoxic effects. Approximately 10% of patients treated with doxorubicin will develop potentially life-threatening cardiotoxicity up to 10 y after treatment (*4*), with higher cumulative doses increasing risk dramatically (*5*). Of those who develop congestive heart failure, mortality is approximately 50% (*6,7*).

Cardiotoxicity is currently routinely monitored by echocardiography or multigated acquisition scanning, typically defined as a 10% or higher reduction of left ventricular ejection fraction (*3,8*). However, such loss of contractile function typically indicates significant irreversible myocardial injury, for which opportunities to intervene or modify treatment are limited (*3,9*).

Measuring evolving cardiac damage at a subcellular level using a molecular imaging approach might provide earlier and more sensitive assessment of cardiotoxicity; however, most of the approaches explored to date are limited in capacity or at a relatively early stage (*10,11*).

Metabolism tracers such as ^{18}F-FDG and ^{11}C-acetate have been investigated; however, cardiac retention is heavily influenced by other parameters, such as dietary substrate availability, which complicate their use (*12*). Tracers more closely related to the mechanisms of cardiotoxicity, such as ^{123}I-metaiodobenzylguanidine, which is sensitive to sympathetic nervous system alterations, have greater promise and have shown a response to doxorubicin treatment preclinically and in patients (*13*). However, slow clearance from blood and significant liver uptake affect their clinical utility (*14*).

Although the exact mechanism of cardiotoxicity by doxorubicin is not fully understood, mitochondrial dysfunction, directly or indirectly, is central to the proposed mechanisms (*4,15,16*). Fluorescent lipophilic cations such as the rhodamine or JC-1 (5,5′,6,6′-tetrachloro-1,1′,3,3′-tetraethylbenzimi-dazolylcarbocyanine iodide) dyes have been used for many years to report on mitochondrial function in vitro. They accumulate via passive diffusion through cell membranes of mitochondria according to the mitochondrial membrane potential, with PET-labeled derivatives showing good sensitivity in myocardial infarction models (*17*). Our collaborators

Received Feb. 11, 2019; revision accepted May 29, 2019.
For correspondence or reprints contact: Nicholas J. Long, Imperial College London, MSRH, White City Campus, London W12 0BZ, U.K.
E-mail: n.long@imperial.ac.uk
Published online May 30, 2019.

have recently demonstrated the potential of using radiolabeled lipophilic cations to report on doxorubicin-induced mitochondrial dysfunction with ^{99m}Tc-sestamibi for SPECT imaging (*18*). Although proof of concept with SPECT imaging has been demonstrated, PET has significant advantages for this approach in terms of sensitivity and the capacity for 3-dimensional pharmacokinetic analysis.

This study therefore aimed to evaluate our recently developed PET lipophilic cation, [1-(2-^{18}F-fluoroethyl),1*H*[1,2,3]triazole-4-ethylene]triphenylphosphonium bromide (^{18}F-MitoPhos) (*19*), as a cardiac imaging agent. We hypothesize that PET radiolabeled lipophilic cations such as ^{18}F-MitoPhos, which are sensitive to mitochondrial membrane potential alterations and accumulate in cardiac tissue, may allow early detection of doxorubicin-induced cardiotoxicity, potentially before mechanical alterations in cardiac function manifest.

MATERIALS AND METHODS

Animal Husbandry

Animals were group-housed within individually ventilated cages with Aspen grade 6 bedding under a 12 h–12 h light–dark cycle (lights on at 7 AM and off at 7 PM) at set temperature and humidity ranges of 19°–23°C and 45%–65%, respectively. Food and water were available ad libitum, and environmental enrichment was provided.

Animal Procedures

All animal procedures were performed in accordance with the United Kingdom Home Office Animals (Scientific Procedures) Act of 1986 and European Union directive 2010/63/EU. The procedures were reviewed by independent ethics committees (Imperial College London and King's College London). All animals were sourced from Charles River.

Radiopharmaceutical Preparation

^{18}F-MitoPhos was produced in greater than 99% radiochemical purity and molar activity of 24.6 ± 18.3 GBq/μmol by a fully automated 2-step radiosynthesis process, adapted from a previously reported methodology (Fig. 1) (*18,20*). ^{18}F-fluorobenzyltriphenylphosphonium (^{18}F-FBnTP) was produced in greater than 99% radiochemical purity and specific activity of 15.0 ± 12.6 GBq/μmol in a fully automated 4-step radiosynthesis, modified from a previously reported procedure (Fig. 1) (*21*). ^{99m}Tc-sestamibi was prepared from commercial cold kits (Mallinckrodt Pharmaceuticals) reconstituted with saline (100 MBq/mL) from a ^{99}Mo/^{99m}Tc generator and supplied by the radiopharmacy of St. Thomas' Hospital, King's College, London, U.K.

Langendorff Heart Perfusion

To investigate tracer response to decreased mitochondrial membrane potential, uptake and kinetic modeling of ^{18}F-MitoPhos was compared with that of the SPECT lipophilic cardiac tracer ^{99m}Tc-sestamibi in male Wistar rat hearts (n = 4–6 per group, 300–330 g) on a triple-γ-detection Langendorff perfusion setup, previously described (*22,23*). Tracers were compared under normoxic control perfusion and in hearts treated with the mitochondrial membrane potential uncoupler carbonyl cyanide 3-chlorophenylhydrazone (CCCP).

After intraperitoneal injection of pentobarbital, hearts were excised from male Wistar rats and cannulated onto a Langendorff perfusion rig. Hearts were perfused with modified Krebs–Henseleit buffer (37°C gassed with 95% O_2/5% CO_2) at a constant flow rate of 14 mL/min. Cardiac tracer retention and washout were monitored throughout each experiment using GinaSTAR software (Raytest Ltd, UK) via the triple-γ-detection system, whereas cardiac contractile function was monitored with an intraventricular balloon connected to a Powerlab system (AD Instruments Ltd) running Labchart software (AD Instruments Ltd). After a stabilization period of 20 min, CCCP (at a final concentration of 300 nmol/L) or vehicle was infused into the aortic cannula via a side arm. After 25 min, a bolus of radiotracer (~1 MBq, 50–100 μL) was injected into the arterial line. Cardiac radiotracer uptake was recorded and decay-corrected, and the exponential washout component was calculated from least-squares fit of data from 2 min after injection.

Ex Vivo Biodistribution

Male Sprague–Dawley rats (300–500 g; n = 3 per time point) were anesthetized, and ^{18}F-MitoPhos or ^{18}F-FBnTP (5.1 ± 1.3 MBq) was administered intravenously. Animals were culled at 5, 15, 30, or 60 min after administration, tissues were collected, and radioactivity was measured via a γ-counter (Wizard).

The distribution of radioactivity in tissue and plasma is expressed as mean SUV, where SUV = [(percentage injected dose per gram of tissue) × (body weight of the animal in grams)]/100.

Metabolite Analysis

Blood samples were collected 5, 10, 20, 40, and 60 min after tracer administration (n = 3 per time point). Proteins were precipitated from plasma with acetonitrile (1:1 plasma-to-acetonitrile ratio) and centrifuged. High-performance liquid chromatography analysis of the supernatant allowed the parent fraction to be determined.

Dynamic PET/CT Cardiac Scanning

The animals were anesthetized, and venous and arterial angiocatheters were inserted for radiotracer injection and periodic blood sampling, respectively. Selected regions of interest were drawn over the heart and used to generate the time–activity curves.

In Vivo Procedures

All in vivo procedures were carried out under anesthesia (2%–3% isoflurane in air, 1 L/min), and animal body temperature was maintained by heating mats, with rectal probe feedback. For dynamic PET/CT cardiac scanning, the animals were placed within the central bore of a Siemens Inveon PET/CT scanner with the field of view over the heart. A CT scan was conducted for attenuation correction before injection of radiotracer and acquisition of the dynamic PET data (60 min). Radiopharmaceuticals were administered via direct puncture of the tail vein. At the end of the protocol, animals were killed via exsanguination under deep anaesthesia (4% isoflurane in air, 1 L/min), and tissues were collected in ice-cold saline and weighed. Radioactivity was measured via a γ-counter (Wizard). Dynamic scan data were histogrammed (10 frames, 3 s; 6 frames, 5 s; 8 frames, 30 s; 5 frames, 60 s; 6 frames, 300 s; and 2 frames, 600 s) and reconstructed (2-dimensional filtered backprojection). One animal within the 10 mg/kg group in the doxorubicin study was excluded because of a failed intravenous injection; this data point was not replaced.

In Vivo Intraanimal Variability

Sprague–Dawley rats (n = 4, 408 ± 95 g) underwent 60-min dynamic PET/CT scans with injection of ^{18}F-MitoPhos (6.2 ± 2.0 MBq). After 48 h, the animals were scanned a second time with ^{18}F-MitoPhos (7.2 ± 1.2 MBq). Cardiac SUV from 30 to 60 min was determined from the dynamic scan time–activity curve of the left ventricle and was used to calculate variability.

Ex Vivo Analysis

Metabolite Quantification. Blood samples were periodically collected (5, 10, 20, 40, and 60 min, n = 3 per time point). Proteins were precipitated from plasma with acetonitrile (1:1) and centrifugation at 12,000*g* for 5 min. Ninety percent acetonitrile:10% 50 mM ammonium formate, pH 4, at 5 mL/min was used as the mobile phase, with a

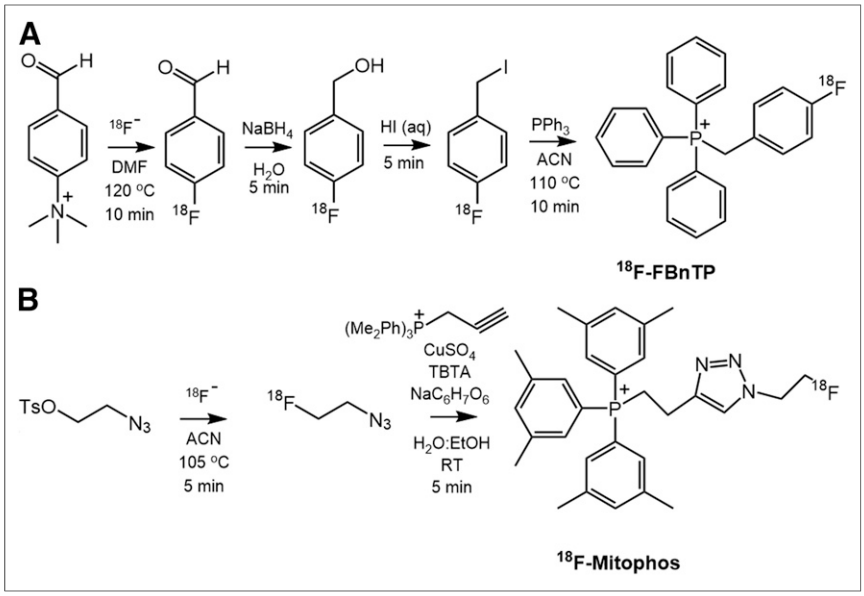

FIGURE 1. Radiosynthetic pathway for PET tracers: ^{18}F-FBnTP (A) and ^{18}F-MitoPhos (B). ACN = acetonitrile; DMF = dimethylformamide; RT = room temperature; TBTA = tris(benzyltriazolylmethyl)amine.

Phenomenex Prodigy semipreparative octadecylsilyl-3 column (10 μm, 250 × 10 mm). The typical activity recovery from high-performance liquid chromatography was more than 90%.

Malondialdehyde Quantification. Left ventricular tissue from the apex of the heart was homogenized in ice-cold 20 mM Tris-HCl buffer, pH 7.4, in a 1:10 ratio before samples were briefly sonicated. Homogenate was centrifuged at 3,000*g* for 10 min at 4°C, and the supernatant was removed for analysis. Two hundred microliters of tissue homogenate were added to 650 μL of 10.3 mM *N*-methyl-2-phenyl-indole in acetonitrile and stirred in a vortex mixer for 3–4 s. One hundred fifty microliters of HCl, 37 %, were added, and samples were incubated at 45°C for 60 min. The samples were cooled in ice and centrifuged before 3 × 200 μL aliquots per sample were transferred to a 96-well plate for reading (absorbance, 586 nm). A standard curve from 1.25 to 40 nM malondialdehyde was used for quantification ($R^2 > 0.999$).

Acute In Vivo Doxorubicin Cardiotoxicity Model

Sprague–Dawley rats received slow, continuous intravenous infusion of doxorubicin (10, 15, or 20 mg/kg) over 1 h. The rats were monitored for signs of adverse effects over 48 h. At 48 h after doxorubicin infusion, the rats were placed under terminal anesthesia and ^{18}F-MitoPhos (6.3 ± 1.7 MBq) was injected intravenously. A subset of rats (n = 3 and 4 for the 15 and 20 mg/kg groups, respectively) underwent dynamic PET/CT, with time–activity curve generation over the left ventricle. Target tissue activity was measured with a γ-counter 60 min after injection; cardiac tissue and blood plasma were frozen for further analysis.

Cardiotoxicity Biomarker Analysis

Plasma collected at the end of the protocol was analyzed for cardiac troponin-I levels (ultrasensitive rat cardiac troponin-I enzyme-linked immunosorbent assay; Life Diagnostics). Samples were thawed to ambient temperature, and enzyme-linked immunosorbent assay was performed according to the manufacturer's instructions, with adaptations of the standard curve to increase sensitivity for lower doses. A standard curve from 19.5 to 625 pg of rat cardiac troponin-I per milliliter was used for quantification ($R^2 > 0.999$).

Levels of malondialdehyde were evaluated in cardiac muscle tissue as a biomarker of oxidative stress. Malondialdehyde was extracted from left ventricular tissue as previously described (*24*). Each sample was transferred to a 96-well plate for reading and was measured in triplicate (absorbance, 586 nm). A standard curve from 1.25 to 40 nmol of malondialdehyde per milliliter was used for quantification ($R^2 > 0.999$).

Hematoxylin- and eosin-stained longitudinal sections of ventricle from doxorubicin-treated rats were histologically assessed. Fresh-frozen cardiac tissue was sectioned (10 μm) using a cryostat and thaw-mounted onto SuperFrost slides. Staining was performed by fixing the tissue with Clarkes solution (3:1 v/v EtOH:glacial acetic acid). Slides were incubated with hematoxylin solution, differentiated in 1% HCl, and then submerging in eosin solution (aqueous, 1%). Tissue was then dehydrated in EtOH (85%, 100%, 100%), cleared in xylene, and allowed to dry before the application of distyrene–plasticizer–xylene medium. Myocardial damage (n = 3 sections per heart, n = 4 hearts per group) was assessed by 2 independent researchers masked to the treatment groups using a scoring system similar to that reported by Erboga et al. (*25*). Randomly selected cardiac sections were imaged and assessed for signs of myocardial damage, namely myofibrillar

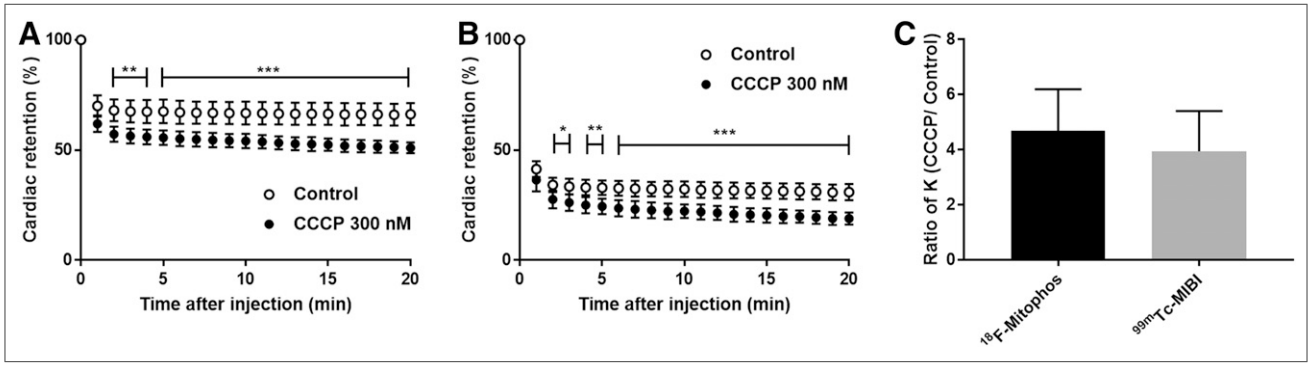

FIGURE 2. (A and B) Cardiac retention of percentage injected dose of ^{18}F-MitoPhos (A) and ^{99m}Tc-sestamibi (B) in Langendorff-perfused hearts in control and CCCP (300 nM)-treated animals. (C) Relative increase in heart washout rate (K) for ^{18}F-MitoPhos and ^{99m}Tc-sestamibi. Statistical analysis was 2-way ANOVA and Dunnett post hoc analysis (A and B) and 2-tailed t test (C). *$P < 0.05$. **$P < 0.01$. ***$P < 0.001$.

loss, cytoplasmic vacuolization, myocardial disorganization, inflammatory cell infiltration, and hemorrhages, using a score of 0 (no damage), 1 (mild damage), 2 (moderate damage), or 3 (severe damage).

Statistical Analysis

Statistical analysis was performed using an unpaired *t* test, 1-way ANOVA with Dunnett post hoc analysis, or 2-way ANOVA with Dunnett post hoc analysis, where appropriate (GraphPad Prism 7 software). All graphs and values are represented as average ± SD. Differences between data sets were deemed statistically significant when the observed confidence interval had a P value of less than 0.05.

RESULTS

In Vitro Analysis on Langendorff Perfused Hearts

Infusion of CCCP (300 nM) into isolated perfused hearts invoked a significant increase in left ventricular end-diastolic pressure, from 6.9 ± 2.3 to 67.5 ± 10.0 mm Hg, and a significant decrease in left ventricular developed pressure, from 122.4 ± 11.1 to 37.7 ± 17.1 mm Hg versus control experiments, at 65 min after perfusion (Supplemental Fig. 1; supplemental materials are available at http://jnm.snmjournals.org). Cardiac time–activity profiles were measured from the heart-orientated γ-detector, for both ^{18}F-MitoPhos and ^{99m}Tc-sestamibi (Figs. 2A and 2B). In control hearts, ^{18}F-MitoPhos exhibited an average single-pass extraction and retention of 66% ± 5% ($n = 5$) of the injected spike at 20 min after injection, in comparison to ^{99m}Tc-sestamibi, which showed 31% ± 4% ($n = 5$) retention. In control hearts, the kinetic washout rate from 2 min after injection for ^{18}F-MitoPhos and ^{99m}Tc-sestamibi was $1.1 \times 10^{-3} \pm 3 \times 10^{-4}$ and $4.5 \times 10^{-3} \pm 1.0 \times 10^{-3}$ percentage injected dose/min, respectively (Supplemental Fig. 1). On treatment with CCCP, both ^{18}F-MitoPhos ($n = 4$) and ^{99m}Tc-sestamibi ($n = 6$) showed a significant decrease in retention from 2 min after injection, which was maintained throughout (15% and 12% of injected dose, respectively, by the end of the protocol) (Figs. 2A and 2B). A significant increase in washout rate was observed for both tracers in hearts treated with CCCP (Supplemental

TABLE 1
Selected Ex Vivo Biodistribution Data for ^{18}F-FBnTP and ^{18}F-MitoPhos and Heart-to-Tissue Ratios

Tissue	5 min	15 min	30 min	60 min
^{18}F-FBnTP				
Blood	0.12 (0.22)	0.16 (0.06)	0.12 (0.06)	0.04 (0.01)
Plasma	0.56 (0.51)	0.08 (0.06)	0.05 (0.04)	0.02 (0.00)
Muscle	0.30 (0.12)	0.22 (0.12)	0.21 (0.04)	0.34 (0.14)
Spleen	5.63 (0.28)	4.58 (1.22)	3.17 (1.65)	2.49 (0.76)
Liver	3.71 (0.93)	3.57 (0.65)	3.58 (1.06)	3.59 (0.73)
Adrenals	6.87 (9.16)	9.84 (1.74)	11.33 (5.33)	7.00 (2.49)
Kidney	17.57 (5.27)	30.08 (3.81)	32.24 (3.44)	25.81 (5.92)
Lung	2.09 (0.38)	2.03 (0.12)	2.09 (0.27)	1.63 (0.47)
Heart	7.42 (0.43)	7.32 (0.69)	7.93 (2.45)	6.75 (1.54)
Brain	0.07 (0.03)	0.05 (0.01)	0.06 (0.02)	0.03 (0.01)
Heart-to-plasma	13.2 (12.0)	95.6 (70.9)	153.1 (135.2)	422.7 (142.5)
Heart-to-lung	3.6 (0.7)	3.6 (0.4)	3.8 (1.3)	4.1 (1.5)
Heart-to-liver	2.0 (0.5)	2.1 (0.4)	2.2 (0.9)	1.9 (0.6)
^{18}F-MitoPhos				
Blood	0.35 (0.17)	0.16 (0.02)	0.14 (0.02)	0.06 (0.02)
Plasma	0.19 (0.11)	0.06 (0.01)	0.07 (0.02)	0.02 (0.01)
Muscle	0.30 (0.04)	0.22 (0.02)	0.24 (0.06)	0.22 (0.06)
Spleen	6.67 (1.87)	6.04 (0.36)	7.28 (0.55)	4.231 (0.83)
Liver	3.91 (0.69)	2.25 (0.30)	1.53 (0.30)	0.463 (0.12)
Adrenals	12.50 (4.52)	11.32 (1.31)	21.16 (6.47)	14.30 (4.25)
Kidney	20.77 (1.63)	17.76 (0.28)	21.69 (1.37)	18.64 (4.57)
Lung	2.36 (0.15)	2.97 (1.42)	1.43 (0.25)	1.37 (0.36)
Heart	5.40 (0.61)	4.60 (0.32)	5.17 (0.56)	5.17 (0.86)
Brain	0.08 (0.01)	0.07 (0.00)	0.06 (0.01)	0.05 (0.01)
Heart-to-plasma	28.3 (16.6)	82.2 (15.7)	95.7 (36.9)	303.9 (185.8)
Heart-to-lung	2.3 (0.3)	1.6 (0.7)	3.6 (0.7)	3.8 (0.6)
Heart-to-liver	1.4 (0.5)	2.0 (0.2)	3.4 (0.8)	11.2 (1.2)

Data are average SUV (followed by SD in parentheses) determined by γ-counter measurement for each time point/min.

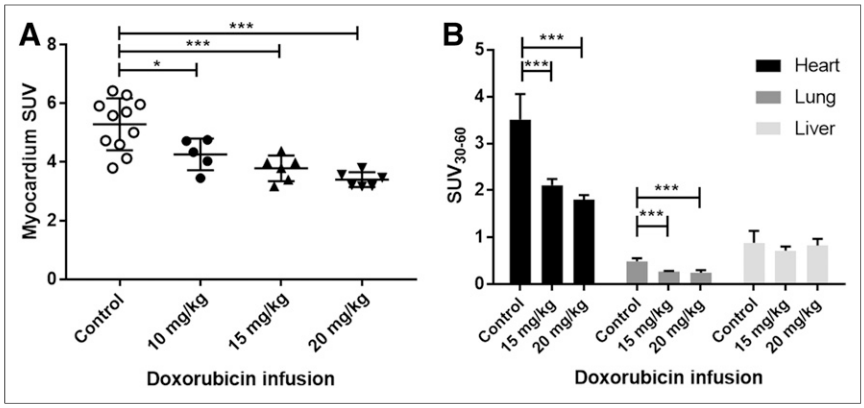

FIGURE 3. Uptake of ^{18}F-MitoPhos in control and doxorubicin-treated animals (mean ± SD). (A) Ex vivo biodistribution of collected cardiac tissue (60 min after injection). (B) Average SUV from 30 to 60 min from left ventricle, lung, and liver time–activity curve, derived from dynamic PET/CT scan. Statistical analysis was 1-way ANOVA and Dunnett post hoc analysis. *$P < 0.05$. ***$P < 0.001$.

Fig. 2), with relative increases of 469% ± 150% and 395% ± 146% for ^{18}F-MitoPhos and ^{99m}Tc-sestamibi, respectively (Fig. 2C).

Ex Vivo Biodistribution of ^{18}F-MitoPhos and ^{18}F-FBnTP

Ex vivo tissue biodistribution and image-derived (30–60 min) SUV data for ^{18}F-MitoPhos and ^{18}F-FBnTP are shown in Table 1. There was no substantial bone uptake, alongside good metabolic stability of ^{18}F-MitoPhos in vivo, with 40% of the parent compound still present in plasma at 60 min after injection (Supplemental Table 1; Supplemental Fig. 3). In accordance with the isolated-heart experimental results, fast uptake and high retention of ^{18}F-MitoPhos were observed in the myocardium of healthy animals, with an average SUV from ex vivo biodistribution of 5.40 ± 0.61 at 5 min after injection and 5.17 ± 0.86 at 60 min. Rapid clearance of ^{18}F-MitoPhos from the plasma, liver, and lungs was observed, with relative heart-to-tissue ratios of 303.9 ± 136.0, 11.2 ± 1.2, and 3.8 ± 0.6, respectively, at 60 min. Distinction of the entire myocardium from all surrounding tissues was apparent in PET-derived images. Intraanimal variability data for ^{18}F-MitoPhos (Supplemental Fig. 4) showed good cardiac uptake repeatability, with an average image-derived cardiac SUV divergence of 8.0% ± 4.3% from baseline scans.

^{18}F-FBnTP showed a biodistribution similar to that of ^{18}F-MitoPhos, with higher uptake in the heart (SUV, 7.42 ± 0.43 at 5 min via ex vivo biodistribution) and rapid clearance from the bloodstream (Table 1). High liver uptake and retention were observed, with consistent heart-to-liver ratios of around 2 throughout the 60-min protocol.

Acute Doxorubicin Treatment Model

Progressive weight loss was observed over the 48-h period for every doxorubicin treatment group, with the 15 mg/kg doxorubicin group showing the greatest weight loss, 7.0% ± 1.5%. No severe adverse effects, as defined by 2 or more persistent signs of ill health, or unscheduled deaths, were encountered throughout the acute experiment (Supplemental Table 2). Ex vivo tissue biodistribution data support a significant, dose-dependent decrease in cardiac retention at 60 min after ^{18}F-MitoPhos injection in all doxorubicin-treated groups, with SUV decreased from 5.3 ± 0.9 (control) to 3.4 ± 0.3 (20 mg/kg dose of doxorubicin) ($P < 0.001$) (Fig. 3A). A strong correlation with cardiac SUV derived from the dynamic scan data (Figs. 3B and 4) was observed, with a decrease in left ventricular cardiac SUV (30–60 min) from 3.5 ± 0.5 in the control group to 1.8 ± 0.1 ($P < 0.001$) in the 20 mg/kg doxorubicin group. Image-derived myocardial time–activity curves showed a significant alteration between the control and doxorubicin-treated groups for myocardium and lung (Fig. 5; Supplemental Fig. 6). No significant alterations in SUV were observed for liver, kidney, blood, or plasma by ex vivo biodistribution across treatment groups (Supplemental Fig. 5).

Biomarker and Histologic Assessment of In Vivo Doxorubicin-Induced Cardiac Damage

Cardiac troponin-I levels in the plasma 48 h after doxorubicin dosing were below the limit of detection for the assay (39 pg/mL) for every sample in each treatment group. No significant differences in malondialdehyde concentration were detected for cardiac tissue collected at the end of the protocol across all groups (Supplemental Fig. 7). Histologic assessment of cardiac damage showed a substantial increase in semiquantitative damage between control group and doxorubicin-treated groups (Table 2). Typical examples of cardiac sections are displayed in Supplemental Figure 8.

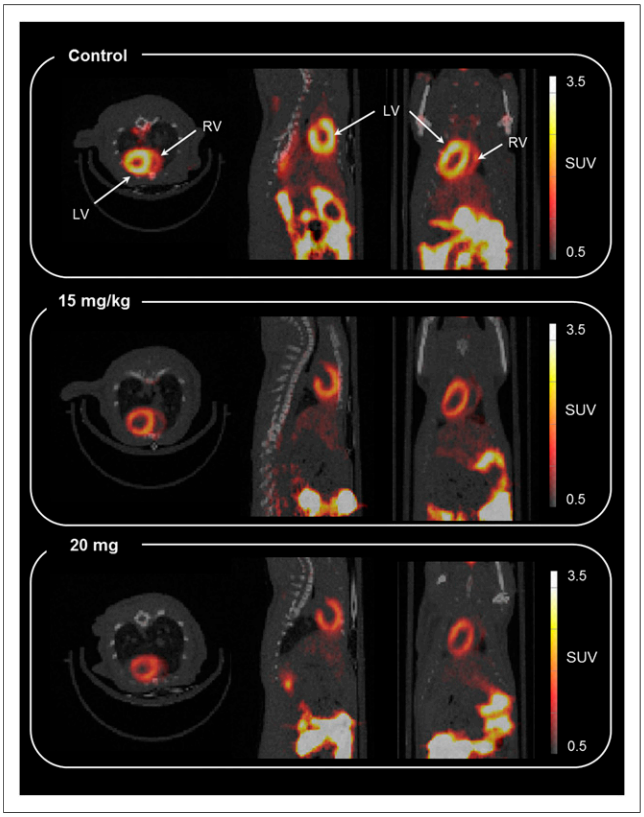

FIGURE 4. Representative axial, sagittal, and coronal coregistered PET/CT image (summed from 30 to 60 min) for ^{18}F-MitoPhos in Sprague–Dawley rats 48 h after doxorubicin dose. Shown are control (top), 15 mg/kg (middle), and 20 mg/kg (bottom). LV = left ventricle; RV = right ventricle.

TABLE 2
Histologic Assessment of Hematoxylin- and Eosin-Stained Tissue Sections of Control and Doxorubicin-Treated Myocardium

	Assessor 1		Assessor 2	
Dose	Average median	Range	Average median	Range
Control	0	0–1	0.5	0–2
10 mg/kg	2	0–3	2.5	0–3
15 mg/kg	2.5	1–3	2.75	2–3
20 mg/kg	2.25	1–3	2.5	1–3

Average median denotes median score of each heart (n = 3 sections) averaged over treatment group. Range denotes total range of sections within treatment group.

DISCUSSION

The long-term cardiotoxic side effects of chemotherapy are becoming increasingly important as cancer detection and survival rates increase. The current methods for cardiotoxicity monitoring rely on structural or mechanical cardiac dysfunction at late stages, when irreversible damage has already occurred and the optimal window for intervention has passed. Research into radiolabeled tracers as potential early identifiers of cardiotoxicity show some potential, but the tracers investigated to date have various limitations. Here, we showed that ^{18}F-MitoPhos has a favorable pharmacokinetic profile for cardiac imaging and is responsive to doxorubicin-induced cardiotoxicity in an acute rodent model.

Historically, radiolabeled lipophilic cations have long been used as myocardial perfusion imaging agents, based on the assumption that their rapid sequestration into cardiac mitochondria is primarily limited by their delivery (*26,27*). However, more recently, the repurposing of the approach to report on mitochondrial membrane potential itself is becoming of interest. Several recent preclinical imaging studies have investigated the potential of using PET radiolabeled lipophilic cation tracers in myocardial infarction models (*17,28,29*), as well as for the quantification of cardiotoxicity by SPECT imaging (*18*). To directly compare the in vivo performance of ^{18}F-MitoPhos with that of another lipophilic cation, we chose ^{18}F-FBnTP as the only PET lipophilic cation agent to be translated into humans.

In the Langendorff perfusion heart model, cardiac retention of ^{18}F-MitoPhos in control perfused hearts was more than double that of ^{99m}Tc-sestamibi, with a higher first-pass extraction and a 4-times-slower washout rate from 2 min after injection. This finding indicates that cardiac uptake of ^{18}F-MitoPhos in vivo will likely be higher than that of ^{99m}Tc-sestamibi and retained longer. Both tracers exhibited significant washout in response to mitochondrial depolarization with the ionophore CCCP, indicating their potential to report on mitochondrial dysfunction in vivo.

Our in vivo pharmacokinetic and biodistribution studies confirmed high uptake and stable retention of both ^{18}F-MitoPhos and ^{18}F-FBnTP in the myocardium and efficient washout from blood. ^{18}F-MitoPhos showed efficient washout from the liver, with heart-to-liver ratios of more than 11 by 60 min, whereas for ^{18}F-FBnTP this ratio remained at 2 throughout, in line with previously published studies (*30*). Because of the proximity of the heart to the liver, high hepatic retention can affect a tracer's usefulness in cardiac imaging, with estimations of SUV in the cardiac apex becoming problematic. In human studies this is a major issue for many cardiac tracers, including ^{18}F-FBnTP, for which ratios are substantially lower in humans than in rodents (<0.2) (*31*). As such, the rapid clearance from the liver that ^{18}F-MitoPhos displays may be a significant advance over currently used agents, warranting further investigation into its use as a PET cardiac perfusion imaging agent.

In this study, a single acute doxorubicin dose was applied to investigate the ability of ^{18}F-MitoPhos to image cardiac tissue damage. To our knowledge, ^{18}F-MitoPhos is the first agent to characterize a PET radiolabeled lipophilic cation for imaging doxorubicin-induced cardiotoxicity. ^{18}F-MitoPhos showed a significant, dose-dependent decrease in cardiac uptake in animals treated with doxorubicin, with left ventricular retention decreasing to almost 50% of the value in controls on dynamic scan data. These results were obtained before detectable plasma levels of the cardiotoxicity biomarker cardiac troponin-I had accrued or significant alterations in cardiac malondialdehyde had occurred.

The lack of biomarker alteration observed in this study is in line with other acute doxorubicin models in the literature. Biomarker alterations are generally observed only after a longer time, 72–96 h (*24,32*), or with higher doxorubicin doses over 48 h (*25,33,34*). However, in our model, histologic assessment of cardiac tissue detected an increase in tissue damage, indicating that mitochondria or mitochondrial membrane potential may be compromised in the early stages of cardiotoxicity and that changes seen with ^{18}F-MitoPhos may allow early detection of cardiotoxicity. Another possibility is a reduction in blood flow due to cardiac atrophy, which has been seen in humans and rodents after prolonged exposure to doxorubicin (*35,36*). Although we cannot definitively rule out this effect as a contributor, a similar doxorubicin study showed no response in the perfusion tracer ^{99m}Tc-*N*-ethoxy-*N*-ethyl dithiocarbamatonitrito, implying no alteration in perfusion, but showed a significant decrease in ^{99m}Tc-sestamibi (also a lipophilic cation) (*18*). The lack of comparison to other perfusion tracers is, however, a limitation of the study. Although the initial data presented here on ^{18}F-MitoPhos show promise, additional studies are required. Chronic models more representative of clinical procedures would

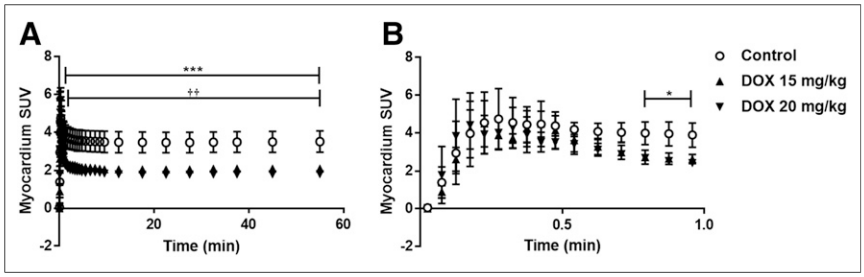

FIGURE 5. Time–activity curves (average SUV ± SD) for ^{18}F-MitoPhos in Sprague–Dawley rats for left ventricle. SUVs are displayed over duration of scan (A) and for first minute (B). Significant decrease in cardiac uptake for both 15 mg/kg and 20 mg/kg dose in myocardium is observed. Statistical analysis was 2-way ANOVA and Dunnett post hoc analysis. ***$P < 0.001$ for control compared with doxorubicin (DOX), 20 mg/kg. ††$P < 0.01$ for control compared with doxorubicin, 15 mg/kg.

allow meaningful comparison to echocardiography techniques and assessment of clinical translation potential.

CONCLUSION

We have reported the potential of the radiolabeled lipophilic cation PET tracer ^{18}F-MitoPhos for imaging evolving mitochondrial cardiotoxicity. ^{18}F-MitoPhos showed improved pharmacokinetic characteristics over clinically used radiolabeled lipophilic cations, for the purposes of cardiac imaging, with fast washout from blood and liver and stable retention in the myocardium. We also found a significant dose response of ^{18}F-MitoPhos cardiac uptake to an acute doxorubicin dose 48 h beforehand. These results show that ^{18}F-MitoPhos is a promising agent for imaging doxorubicin-induced cardiotoxicity, with potential as an early diagnostic tool. Our results justify further studies on ^{18}F-MitoPhos in chronic-toxicity models.

DISCLOSURE

A CASE award was funded by the Medical Research Council (U.K.) and Imanova Ltd. to Stuart McCluskey and by the Biotechnology and Biological Sciences Research Council (U.K.), GSK, and Imanova Ltd. to Anna Haslop. No other potential conflict of interest relevant to this article was reported.

ACKNOWLEDGMENTS

We thank Drs. Erica Smyth and Roser Farre Garros for assessing cardiac section damage.

KEY POINTS

QUESTION: Is ^{18}F-MitoPhos applicable for imaging mitochondrial dysfunction from acute doxorubicin cardiotoxicity?

PERTINENT FINDINGS: The pharmacokinetic profile of ^{18}F-MitoPhos in rodents is suitable for cardiac imaging, with fast liver clearance—a notable advantage over current in-human lipophilic cation tracers. A significant and dose-responsive decrease in ^{18}F-MitoPhos cardiac uptake was observed on acute doxorubicin treatment. ^{18}F-MitoPhos shows promise as a cardiac imaging agent and warrants further investigation for cardiotoxicity applications.

IMPLICATIONS FOR PATIENT CARE: Early detection of cardiotoxicity may improve chemotherapy morbidity rates.

REFERENCES

1. Siegel RL, Miller KD, Jemal A. Cancer statistics, 2016. *CA Cancer J Clin.* 2016;66:7–30.
2. Blum RH, Carter SK. Adriamycin. *Ann Intern Med.* 1974;80:249–259.
3. Bloom MW, Hamo CE, Cardinale D, et al. Cancer therapy–related cardiac dysfunction and heart failure. *Circ Heart Fail.* 2016;9:e002661.
4. Octavia Y, Tocchetti CG, Gabrielson KL, Janssens S, Crijns HJ, Moens AL. Doxorubicin-induced cardiomyopathy: from molecular mechanisms to therapeutic strategies. *J Mol Cell Cardiol.* 2012;52:1213–1225.
5. Lefrak EA, Pitha J, Rosenheim S, Gottlieb JA. A clinicopathologic analysis of Adriamycin cardiotoxicity. *Cancer.* 1973;32:302–314.
6. Chatterjee K, Zhang J, Honbo N, Karliner JS. Doxorubicin cardiomyopathy. *Cardiology.* 2010;115:155–162.
7. Von Hoff DD, Layard MW, Basa P, et al. Risk factors for doxorubicin-induced congestive heart failure. *Ann Intern Med.* 1979;91:710–717.
8. Cardinale D, Colombo A, Bacchiani G, et al. Early detection of anthracycline cardiotoxicity and improvement with heart failure therapy. *Circulation.* 2015;131:1981–1988.
9. Kongbundansuk S, Hundley WG. Noninvasive imaging of cardiovascular injury related to the treatment of cancer. *JACC Cardiovasc Imaging.* 2014;7:824–838.
10. Jiji RS, Kramer CM, Salerno M. Non-invasive imaging and monitoring cardiotoxicity of cancer therapeutic drugs. *J Nucl Cardiol.* 2012;19:377–388.
11. Bennink RJ, van den Hoff MJ, van Hemert FJ, et al. Annexin V imaging of acute doxorubicin cardiotoxicity (apoptosis) in rats. *J Nucl Med.* 2004;45:842–848.
12. Inglese E, Leva L, Matheoud R, et al. Spatial and temporal heterogeneity of regional myocardial uptake in patients without heart disease under fasting conditions on repeated whole-body ^{18}F-FDG PET/CT. *J Nucl Med.* 2007;48:1662–1669.
13. de Geus-Oei L-F, Mavinkurve-Groothuis AMC, Bellersen L, et al. Scintigraphic techniques for early detection of cancer treatment-induced cardiotoxicity. *J Nucl Med.* 2011;52:560–571.
14. Valdés Olmos RA, ten Bokkel Huinink WW, ten Hoeve RF, et al. Assessment of anthracycline-related myocardial adrenergic derangement by [^{123}I]metaiodobenzylguanidine scintigraphy. *Eur J Cancer.* 1995;31A:26–31.
15. Damiani RM, Moura DJ, Viau CM, Caceres RA, Henriques JAP, Saffi J. Pathways of cardiac toxicity: comparison between chemotherapeutic drugs doxorubicin and mitoxantrone. *Arch Toxicol.* 2016;90:2063–2076.
16. Renu K, VG A, PB TP, Arunachalam S. Molecular mechanism of doxorubicin-induced cardiomyopathy: an update. *Eur J Pharmacol.* 2018;818:241–253.
17. Mou T, Zhang X. Research progress on ^{18}F-labeled agents for imaging of myocardial perfusion with positron emission tomography. *Molecules.* 2017;22:E562.
18. Safee ZM, Baark F, Waters ECT, et al. Detection of anthracycline-induced cardiotoxicity using perfusion-corrected ^{99m}Tc sestamibi SPECT. *Sci Rep.* 2019;9:216.
19. Haslop A, Gee A, Plisson C, Long N. Fully automated radiosynthesis of [1-(2-[^{18}F]fluoroethyl),^{1}H[1,2,3]triazole 4-ethylene] triphenylphosphonium bromide as a potential positron emission tomography tracer for imaging apoptosis. *J Labelled Comp Radiopharm.* 2013;56:313–316.
20. Haslop A, Wells L, Gee A, Plisson C, Long N. One-pot multi-tracer synthesis of novel ^{18}F-labeled PET imaging agents. *Mol Pharm.* 2014;11:3818–3822.
21. Ravert HT, Madar I, Dannals RF. Radiosynthesis of 3-[^{18}F]fluoropropyl and 4-[^{18}F]fluorobenzyl triarylphosphonium ions. *J Labelled Comp Radiopharm.* 2004;47:469–476.
22. Handley MG, Medina RA, Mariotti E, et al. Cardiac hypoxia imaging: second-generation analogues of ^{64}Cu-ATSM. *J Nucl Med.* 2014;55:488–494.
23. Mariotti E, Veronese M, Dunn JT, et al. Assessing radiotracer kinetics in the Langendorff perfused heart. *EJNMMI Res.* 2013;3:74.
24. Poussios D, Andreadou I, Papalois A, et al. Protective effect of a novel antioxidant non-steroidal anti-inflammatory agent (compound IA) on intestinal viability after acute mesenteric ischemia and reperfusion. *Eur J Pharmacol.* 2003;465:275–280.
25. Erboga M, Bozdemir Donmez Y, Sener U, Fidanol Erboga Z, Aktas C, Kanter M. Effect of *Urtica dioica* against doxorubicin-induced cardiotoxicity in rats through suppression of histological damage, oxidative stress and lipid peroxidation. *Electronic J Gen Med.* 2016;13:139–144.
26. Zhang X, Liu XJ, Wu Q, et al. Clinical outcome of patients with previous myocardial infarction and left ventricular dysfunction assessed with myocardial ^{99m}Tc-MIBI SPECT and ^{18}F-FDG PET. *J Nucl Med.* 2001;42:1166–1173.
27. DePuey EG, Rozanski A. Using gated technetium-99m-sestamibi SPECT to characterize fixed myocardial defects as infarct or artifact. *J Nucl Med.* 1995;36:952–955.
28. Madar I, Ravert H, DiPaula A, Du Y, Dannals RF, Becker L. Assessment of severity of coronary artery stenosis in a canine model using the PET agent ^{18}F-fluorobenzyl triphenyl phosphonium: comparison with ^{99m}Tc-tetrofosmin. *J Nucl Med.* 2007;48:1021–1030.
29. Shoup TM, Elmaleh DR, Brownell A-L, Zhu A, Guerrero JL, Fischman AJ. Evaluation of (4-[^{18}F]fluorophenyl)triphenylphosphonium ion: a potential myocardial blood flow agent for PET. *Mol Imaging Biol.* 2011;13:511–517.
30. Madar I, Ravert H, Nelkin B, et al. Characterization of membrane potential-dependent uptake of the novel PET tracer ^{18}F-fluorobenzyl triphenylphosphonium cation. *Eur J Nucl Med Mol Imaging.* 2007;34:2057–2065.
31. Srinivasan S, Muhammad C, Ravert H, et al. Human biodistribution and radiation dosimetry of ^{18}F-fluorobenzyltriphenyl phosphonium [abstract]. *J Nucl Med.* 2012;53(suppl 1):1512.
32. Kwatra M, Kumar V, Jangra A, et al. Ameliorative effect of naringin against doxorubicin-induced acute cardiac toxicity in rats. *Pharm Biol.* 2016;54:637–647.
33. Goyal SN, Mahajan UB, Chandrayan G, et al. Protective effect of oleanolic acid on oxidative injury and cellular abnormalities in doxorubicin induced cardiac toxicity in rats. *Am J Transl Res.* 2016;8:60–69.
34. Saad SY, Najjar TA, Al-Rikabi AC. The preventive role of deferoxamine against acute doxorubicin-induced cardiac, renal and hepatic toxicity in rats. *Pharmacol Res.* 2001;43:211–218.
35. Ferreira de Souza T, Quinaglia A C, Silva T, Osorio Costa F, et al. Anthracycline therapy is associated with cardiomyocyte atrophy and preclinical manifestations of heart disease. *JACC Cardiovasc Imaging.* 2018;11:1045–1055.
36. Willis MS, Parry TL, Brown DI, et al. Doxorubicin exposure causes subacute cardiac atrophy dependent on the striated muscle–specific ubiquitin ligase MuRF1. *Circ Heart Fail.* 2019;12.